ACS OMEGA

http://pubs.acs.org/journal/acsodf

Article

Deciphering the Heterogeneity of the Internal Environment of Hippocampal Neurons during Maturation by Raman Spectroscopy

Xiaodong Kong,[#] Haoyue Liang,[#] Kexuan Zhou, Haoyu Wang, Dai Li, Shishuang Zhang, Ning Sun, Min Gong,* Yuan Zhou,* and Qiang Zhang*

Cite This: *ACS Omega* 2022, 7, 30571−30581

Read Online

ACCESS | Metrics & More | Article Recommendations | Supporting Information

ABSTRACT: Hippocampal neurons are sensitive to changes in the internal environment and play a significant role in controlling learning, memory, and emotions. A remarkable characteristic of the aging brain is its ability to shift from a state of normal inflammation to excessive inflammation. Various cognitive abilities of the elderly may suffer from serious harm due to the change in the neural environment. Hippocampal neurons may have various subsets involved in controlling their internal environment at different stages of development. Developmental differences may eventually result from complex changes in the dynamic neuronal system brought on by metabolic changes. In this study, we used an in vitro hippocampal neuron model cultured in C57BL/6J mice in conjugation with Raman spectroscopy to examine the relative alterations in potential biomarkers, such as levels of metabolites in the internal environment of hippocampal neurons at various developmental stages. The various differentially expressed genes (DEGs) of hippocampal neurons at various developmental stages were simultaneously screened using bioinformatics, and the biological functions as well as the various regulatory pathways of DEGs were preliminarily analyzed, providing an essential reference for investigating novel therapeutic approaches for diseases that cause cognitive impairment, such as Alzheimer's disease. A stable hippocampal neuron model was established using the GIBCO C57BL/6J hippocampal neuron cell line as a donor and in vitro hippocampal neuron culture technology. The Raman peak intensities of culture supernatants from the experimental groups incubated for 0, 7, and 14 days in vitro(DIV) were examined. The GEO database was used to screen for different DEGs associated with various developmental stages. The data was then analyzed using a statistical method called orthogonal partial least squares discriminant analysis (OPLS-DA). The levels of ketogenic and glycogenic amino acids (such as tryptophan, phenylalanine, and tyrosine), lipid intake rate, glucose utilization rate, and nucleic acid expression in the internal environment of hippocampal neurons were significantly different in the 14 DIV group compared to the 0 DIV and 7 DIV groups ($P < 0.01$). The top 10 DEGs with neuronal maturation were screened, and the results were compared to the OPLS-DA model's analysis of the differential peaks. It was found that different genes involved in maturation can directly relate to changes in the body's levels of ketogenic and glycogenic amino acids ($P < 0.01$). The altered expression of the maturation-related genes epidermal growth factor receptor, protein tyrosine kinase 2-beta, discs large MAGUK scaffold protein 2, and Ras protein-specific guanine nucleotide releasing factor 1 may be connected to the altered uptake of ketogenic and glycogenic amino acids and nucleic acids in the internal environment of neurons at different developmental stages. The levels of ketogenic, glycogenic amino acids, and lipid intake increased while glucose utilization decreased, which may be related to mature neurons' metabolism and energy use. The decline in nucleic acid consumption could be connected to synaptic failure. The Raman spectroscopy fingerprint results of relevant biomarkers in conjugation with multivariable analysis and biological action targets suggested by differential genes interpret the heterogeneity of the internal environment of mature hippocampal neurons in the process of maturation, open a new idea for exploring the dynamic mechanism of the exchange energy metabolism of information molecules in the internal environment of hippocampal neurons, and provide a new method for studying this process.

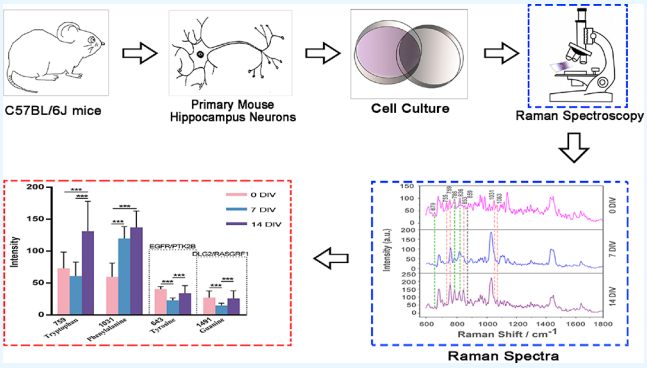

INTRODUCTION

Neurodegenerative diseases are the primary cause of the high morbidity and disability rate among the elderly, resulting in a significant social and economic burden. They are receiving increasing attention as social aging worsens. There is no clear, specific, and reliable laboratory method for their early

Received: July 4, 2022
Accepted: August 11, 2022
Published: August 19, 2022

https://doi.org/10.1021/acsomega.2c04188
ACS Omega 2022, 7, 30571−30581

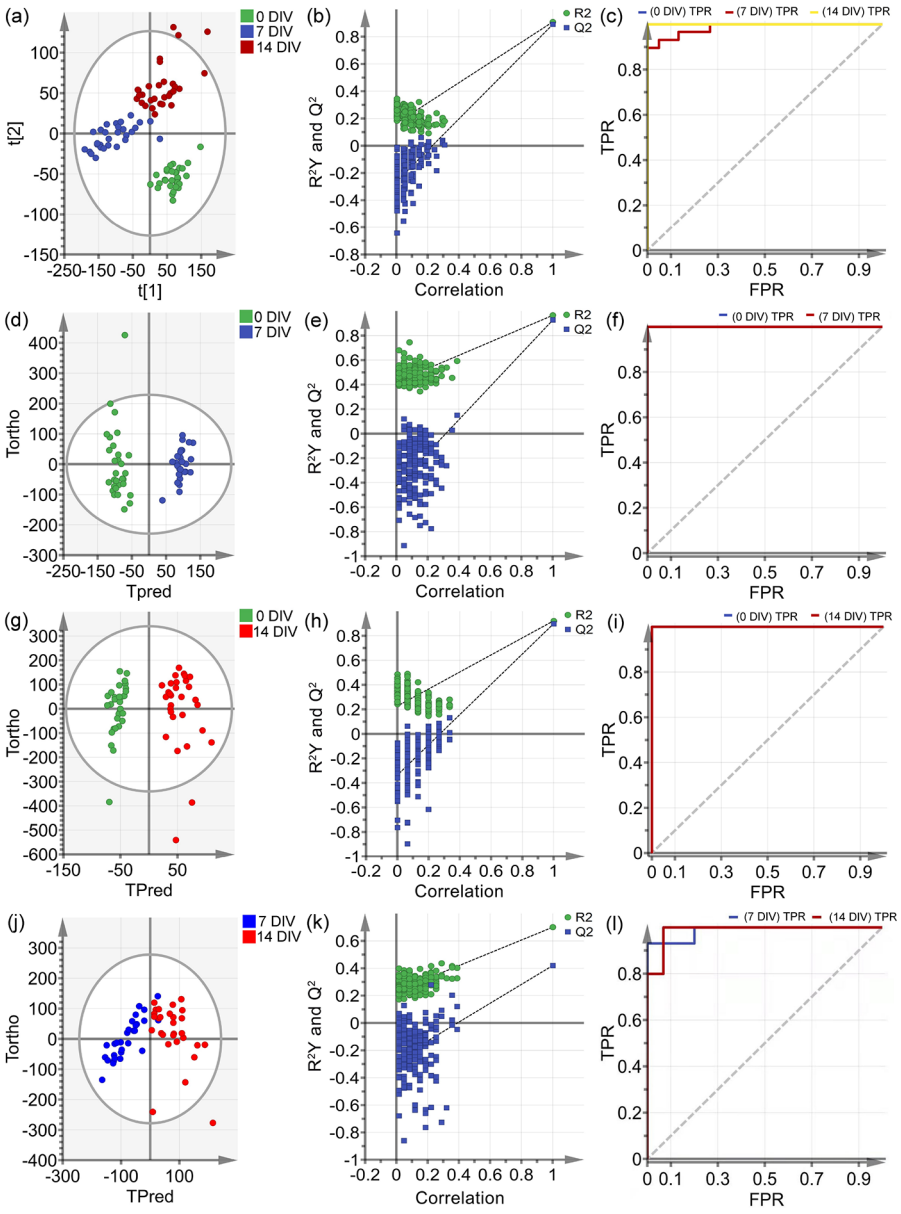

Figure 1. (a) Hippocampal neuron group discrimination score plot using orthogonal partial least squares discriminant analysis (OPLS-DA) discrimination score plots of 0 DIV, 7 DIV, and 14 DIV with Hotelling's 95% confidence ellipse. (b) OPLS model permutation plot of the hippocampal neuron groups at 0 DIV, 7 DIV, and 14 DIV. (c) Hippocampal neuron groups of 0 DIV, 7 DIV, and 14 DIV receiver operating characteristic (ROC) curves. (d) Plot of the OPLS-DA discrimination scores for the groups of 0 DIV and 7 DIV hippocampal neurons using Hotelling's 95% confidence ellipse. (e) Permutation plot of the 0 DIV and 7 DIV hippocampal neuron groups from the OPLS model. (f) ROC curve of the hippocampal neuron groups at 0 DIV and 7 DIV. (g) Plot of the OPLS-DA discrimination scores for the 0 DIV and 14 DIV hippocampal neuron groups using Hotelling's 95% confidence ellipse. (h) Permutation plot of the 0 DIV and 14 DIV hippocampal neuron groups from the OPLS model. (i) Hippocampal neuron groups at 0 DIV and 14 DIV ROC curves. (j) Plot of 7 DIV and 14 DIV hippocampal neuron groups' OPLS-DA discrimination scores using Hotelling's 95% confidence ellipse. (k) Permutation plot of the hippocampal neuron groups from the 7 and 14 DIV OPLS models. (l) ROC curve of the hippocampal neuron groups at 7 DIV and 14 DIV.

diagnosis due to their occult onset, slow development, and complex pathophysiological changes. An optical technique called Raman spectroscopy (RS) of the inelastic light scattering process detects the inelastically scattered light produced by the interaction between light and matter. It provides the chemical fingerprint information of cells, tissues, or biological fluids by detecting the scattered light of molecules. It can quickly and accurately screen for disease susceptibility and incidence. It is applied to the study of biological species that are clinically related. It has numerous potential applications in the pathogenesis and diagnosis of illnesses. Previous research has demonstrated that surface-enhanced Raman scattering technology uses colloids to synthesize silver nanoprobes to detect amyloid precursor proteins in the blood of patients with Alzheimer's disease with high sensitivity and selectivity, and it is free from water interference and non-photobleaching, making RS technology an important research tool for detecting biomarkers of various neurodegenerative diseases. Raman spectroscopy also has the potential for detecting biomarkers of various neurodegenerative diseases.

Ions and nutrients found in extracellular fluid keep cells functioning normally. Therefore, extracellular fluid was referred

https://doi.org/10.1021/acsomega.2c04188
ACS Omega 2022, 7, 30571−30581

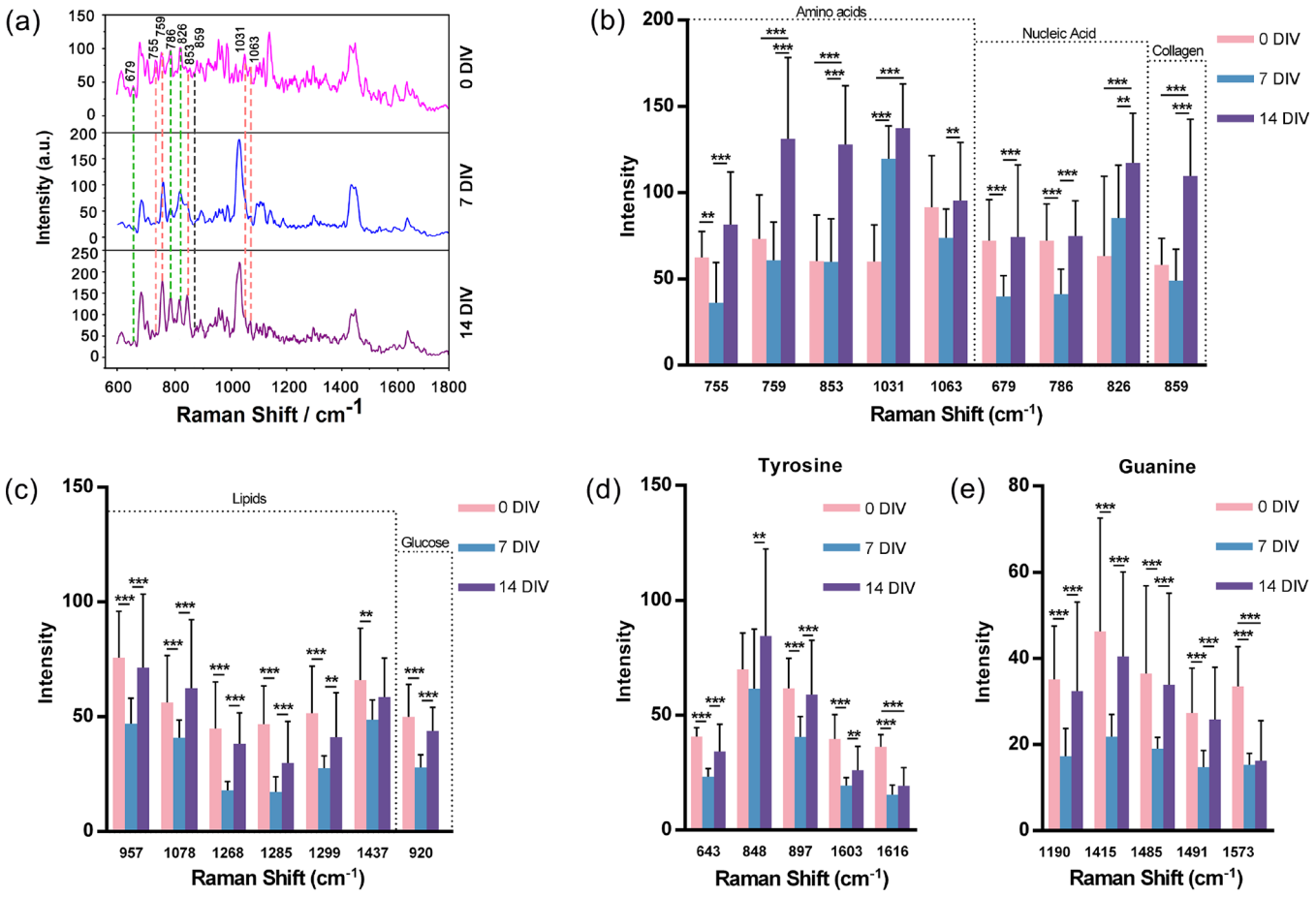

Figure 2. Raman spectroscopy was used to obtain the Raman spectra of the 0, 7, and 14 days in vitro (DIV) hippocampal neuron groups. The peak position (a) found using the orthogonal partial least squares discriminant analysis (OPLS-DA) model is represented by the significant value in the figure. To confirm OPLS-DA, statistical methods were used to obtain the differential peak positions (b); statistical analysis was used to determine the different levels of lipids and sugars in the culture supernatant of hippocampal neurons at 0 DIV, 7 DIV, and 14 DIV (c); and through statistical analysis, it was possible to determine the results of the different peak positions of tyrosine (d) and guanine (e) in the culture supernatant of hippocampal neurons of 0, 7, and 14 DIV. $^{**}P < 0.01$ and $^{***}P < 0.001$. When expressing data, normal distribution-conforming data are expressed as mean ± standard deviation and non-normal distribution-conforming data are expressed as the median of the quartile range.

to as the internal environment of the body by French physiologist Claude Bernard in the 19th century. Neurons differentiate at the end stage and are specific to aging processes. Hippocampal neurons play a very important role in learning, memory, and emotion regulation and are sensitive to changes in the internal environment. Berg et al. have revealed the epigenetic characteristics of hippocampal neurons through a single-cell RNA sequencing analysis, suggesting that hippocampal neurons exhibit high plasticity.[1,2] The internal environment of neurons affects aging by regulating neuronal apoptosis, autophagy, inflammation, and regeneration and repair.[3] The normal brain is heterogeneous and is composed of many specialized cell types. It has a highly accurate electrophysiological behavior, allowing the brain to efficiently manage its energy supply, remove tissue waste, and provide an immune defense.[2] The aging brain loses inflammatory homeostasis, and a pro-inflammatory state sets in. Compared with adult animals, elderly animals exhibit excessive cytokine production and severe cognitive impairment.[4] The change in the neural environment may severely impair cognitive function in the elderly.[5] At various stages of development, neurons may contain subpopulations involved in regulating the internal environment. They can experience metabolic changes and even synaptic failure due to their differences. Target neurons will eventually stop receiving support from surrounding non-specific nerve cells due to physical deterioration, changing the prognosis.

We hypothesize that mature hippocampal neurons have unique energy supply and signal transduction properties based on the characteristics of hippocampal neurons at various developmental stages. It is more challenging to maintain the stable state of the internal environment in neurons at different developmental stages because we assume that they have different capacities for absorbing nutrients and excreting waste products as well as different energy sources needed to maintain normal physiological functions. We cultured hippocampal neurons from C57BL/6J mice and used Raman spectroscopy (working on the principle of inelastic light scattering) to capture the survival environment of hippocampal neurons. Specific biomolecular "fingerprints" reflected the changes in internal environmental substances such as amino acids, nucleic acids, lipids, and glucose in the living environment of neurons at various developmental stages. Combined with gene chip data technology, we downloaded and sorted out biological information related to maturation processes from the gene expression omnibus (GEO) database, performed microarray

https://doi.org/10.1021/acsomega.2c04188
ACS Omega 2022, 7, 30571−30581

analysis, and identified the key genes of hippocampal neurons that are responsible for various developmental stages. Incorporating the biological action targets suggested by multivariable analysis and differential genes with the fingerprint results of relevant biomarkers obtained by RS technology opens a new idea for exploring the dynamic mechanism of information molecule exchange and energy metabolism in the internal environment of hippocampal neurons and offers a new method and idea for quick and inexpensive diagnosis of neurodegenerative diseases (Figure S1).

RESULTS

Identification of Raman Peaks to Distinguish Hippocampal Neurons Cultured for Various Durations. This study examined the Raman spectra of cell supernatants from hippocampal neurons cultured in vitro at different times of 0 DIV, 7 DIV, and 14 DIV. Each group was collected of 29−30 spectrograms. In the experiment, 89 spectrograms were recorded. There were 1208 Raman peak positions with each peak range between 601.26 and 1799.17. This study's main challenge is quickly screening meaningful peaks from multiple peak data. Therefore, we first screen out potentially important biological peaks using the orthogonal partial least squares discriminant (OPLS-DA) multiparameter analysis model. A supervised OPLS-DA model was established using 30, 29, and 30 Raman spectra of the culture medium supernatant of 0, 7, and 14 DIV hippocampal neuron groups, respectively (Figure 1). Figure 2a shows the Raman spectra of the three groups in 600−1800 cm^{-1}. The spectra of 7 DIV and 14 DIV hippocampal neuron groups showed similar morphologies. Therefore, it was necessary to screen further the peaks that can effectively identify 0, 7, and 14 DIV hippocampal neuron groups as potential biomarkers in combination with the classification model established by the OPLS-DA method. For the establishment of the OPLS-DA model, the VIP (VIP > 1.5), correlation coefficient, loadings, and distance from the center in the $V + S$ plot and other relevant parameters were considered (Figure 1 and Figure S4).

The peaks related to amino acids (755, 759, 853, 1031, and 1063 cm^{-1}), nucleic acids (679, 786, and 826 cm^{-1}), and lipids (859 cm^{-1}) obtained by the OPLS-DA model are represented by orange-red, green, and black vertical lines, respectively, in Figure 2a. The peak position attribution of the Raman spectrum is shown in Table S8. The effectiveness of the supervised OPLS-DA model based on Raman spectrum data can be evaluated based on the scoring diagram (Figure 1a,d,g,j), permutation plot (Figure 1b,e,h,k), and ROC plot (Figure 1c,f,i,l). In the figure, the three groups of samples can be distinguished clearly. The 0 DIV and 14 DIV hippocampal neuron groups are located in the positive half-axis of X, and the 7 DIV hippocampal neuron group is located in the negative half-axis of X, reflecting that the three groups have been distinguished. The 14 DIV and 0 DIV groups were located in the positive and negative half-axes of Y, respectively, reflecting that the two types of culture media were distinguished. The results showed that the supervised OPLS-DA method could well distinguish the spectral data of the culture medium of 0, 7, and 14 DIV hippocampal neuron groups, allowing further analysis of the material characteristics of the three groups.[6]

Figure 1d,g,j shows the OPLS-DA score plot of the three models of 0 DIV and 7 DIV hippocampal neuron groups, 0 DIV and 14 DIV hippocampal neuron groups, and 7 DIV and 14 DIV hippocampal neuron groups, respectively. The two groups of samples in the three figures are located on the positive and negative half-axes of X. The sample clustering in the scatter diagram was obvious, reflecting that OPLS-DA could well extract the differential information in the spectrum. The established identification method could identify the differences in the composition of the culture medium samples, and the three models could well identify the two groups of samples in the model (Figure 1d,g,j). The permutation plot was used to judge whether the model was established, and the intercept of Q^2 on the Y axis was negative, indicating that the OPLS-DA model was established and not overfitted (Figure 1b,e,h,k). The ROC plot was used to evaluate the authenticity of the identification method. The closer the area under the curve (AUC) is to 1, the higher the authenticity of the identification method. The ROC curve showed that, in the models of the 0 DIV, 7 DIV, and 14 DIV hippocampal neuron group, AUC (0 DIV) = 1, AUC (7 DIV) = 0.984483, and AUC (14 DIV) = 1 (Figure 1c); in the models of the 0 DIV and 7 DIV hippocampal neuron group, AUC (0 DIV) = 1 and AUC (7 DIV) = 1 (Figure 1f); in the models of the 0 DIV and 14 DIV hippocampal neuron group, AUC (0 DIV) = 1 and AUC (14 DIV) = 1 (Figure 1i); and in the models of the 7 and 14 DIV hippocampal neuron group, AUC (7 DIV) = 0.986207 and AUC (14 DIV) = 0.986207 (Figure 1l). These results suggest the high accuracy of discriminant analysis results.

Figure S4a is the OPLS-DA loading plot, which was used to preliminarily screen the Raman peak positions contributing to the identification model of 0 DIV, 7 DIV, and 14 DIV hippocampal neuron groups. Amino acid (759 cm^{-1}), nucleic acid (786 cm^{-1}), collagen (859 cm^{-1}), and other characteristic peaks play an important role in the identification of the three groups of samples. Figure S4d,g,j are the loading plots of three pairwise combination models. The peak intensity of the protein (1031 and 1063 cm^{-1}) in the 7 DIV hippocampal neuron group was higher than that in the 0 DIV group (Figure S4d). The peak intensities of collagen (859 cm^{-1}), nucleic acid (826 cm^{-1}), and amino acid (759, 853, 1031, and 1063 cm^{-1}) were higher in the 14 DIV hippocampal neuron group than in the 0 DIV group (Figure S4g), while the peak intensities of collagen (859 cm^{-1}), nucleic acid (679 and 786 cm^{-1}), and protein (755, 759, and 853 cm^{-1}) were lower in the 7 DIV hippocampal neuron group than in the 14 DIV hippocampal neuron group (Figure S4j). These results were consistent with the results of subsequent statistical analysis (Figure 2b). Figure S4e,h,k is the VIP diagrams of the three respective pairwise combination models. The number of peaks with a correlation coefficient greater than 0.4 for the comparison of the 7 DIV and 14 DIV hippocampal neuron group, 0 DIV and 14 DIV hippocampal neuron group, and 0 DIV and 7 DIV hippocampal neuron group showed that there might be large material differences between the 14 DIV hippocampal neuron group and the 7 DIV hippocampal neuron group. Raman peaks with VIP > 1.5 have biological significance. After statistical verification, a tryptophan peak (755 and 759 cm^{-1}), tyrosine/proline peak (853 cm^{-1}), and phenylalanine peak (1031 cm^{-1}), nucleic acid peaks (679, 786, and 826 cm^{-1}), and a peak position representing the peak position of collagen material (859 cm^{-1}) were selected as potential markers to distinguish 0 DIV, 7 DIV, and 14 DIV hippocampal neuron groups (Figure 2b).

Validation of Raman Peaks to Distinguish between 7 DIV and 14 DIV Hippocampal Neurons. In verifying the biological peak positions for distinguishing between 7 DIV and

https://doi.org/10.1021/acsomega.2c04188
ACS Omega 2022, 7, 30571−30581

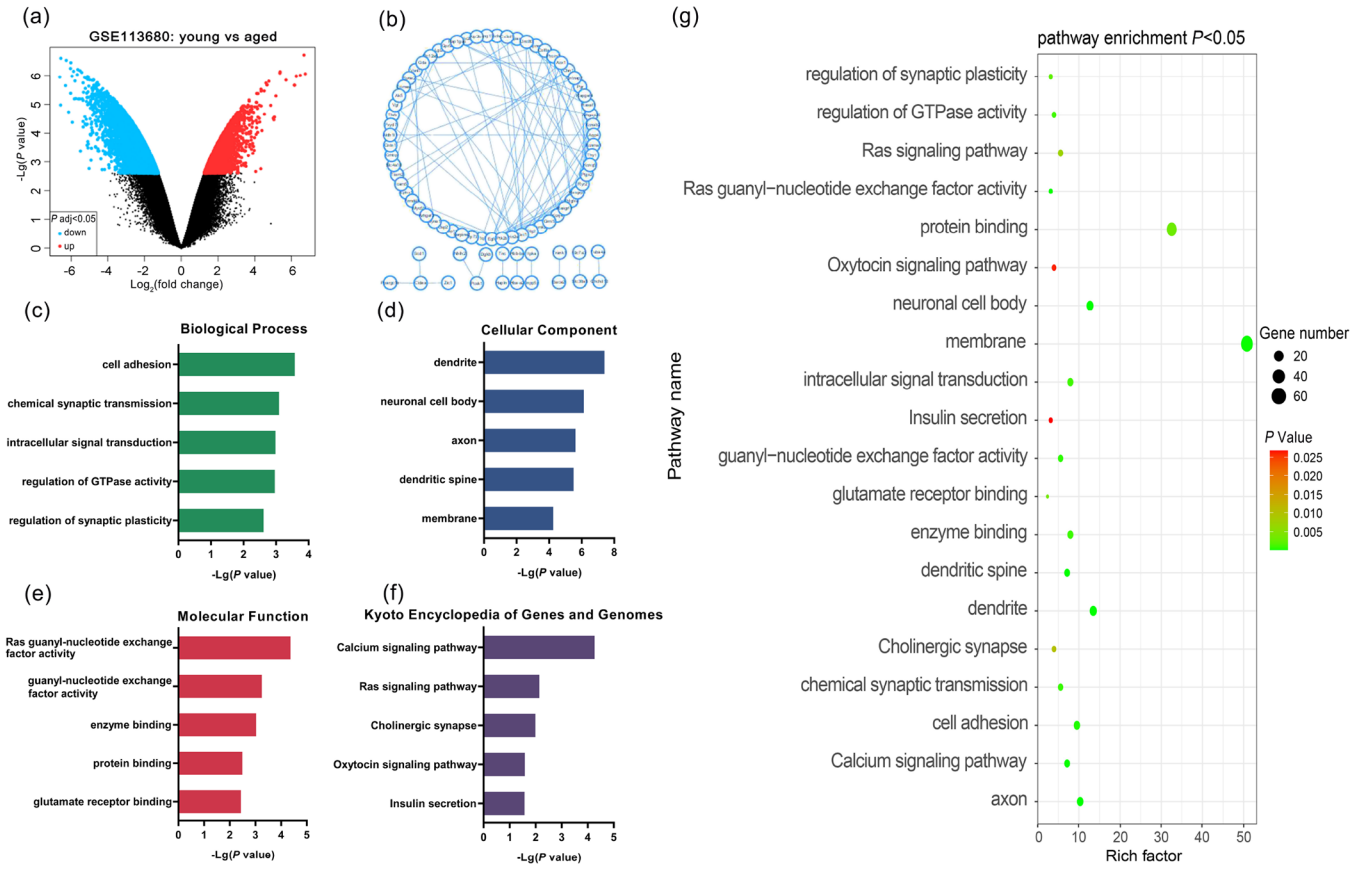

Figure 3. (a) Volcano map of genes significantly differentially expressed between 0 and 15 DIV hippocampal neurons. The fold change is depicted on the *X* axis (logarithmic scale), and the *P* value is displayed on the *Y* axis (logarithmic scale). Each symbol represents a different gene, and the red/blue contrast designates up-/downregulated genes according to various standards (*P* value and fold change threshold). $P < 0.05$ was considered statistically significant. (b) Network diagram of differentially expressed genes' protein−protein interactions. (c) Examining biological processes. (d) Analysis of cell components. (e) Examining the molecular functions. (f) Kyoto Encyclopedia of Genes and Genomes. (g) Bubble diagram of functional enrichment analysis of differentially expressed genes. The larger the bubble, the more genes enriched in this functional pathway, the closer the bubble's color to red, and the higher the significance.

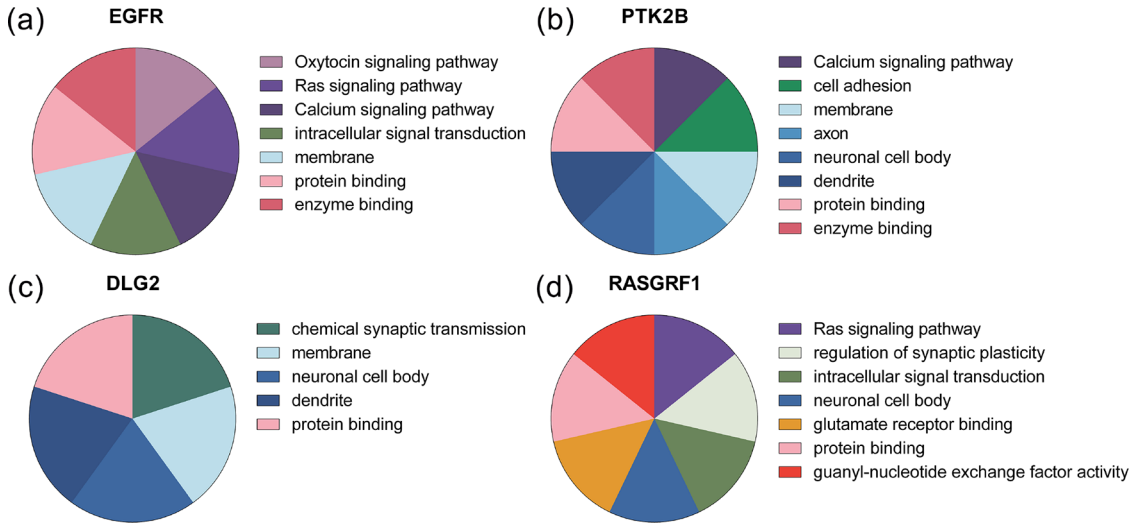

Figure 4. Functional and regulatory signaling pathways of the genes *EGFR* (a), *PTK2B* (b), *DLG2* (c), and *RASGRF1* (d) most likely involved in hippocampal neuronal maturation.

14 DIV hippocampal neurons in the OPLS model, according to the parameter analysis results of VIP greater than 1.5 in the OPLS model, we found that the statistical results were consistent with the peaks in the OPLS model. The statistical results showed that the content of amino acids (755, 759, 853, 1031, and 1063 cm^{-1}) in the culture supernatant of the 14 DIV hippocampal neuron group was significantly higher than that of the 7 DIV hippocampal neuron group ($P < 0.01$). The content

https://doi.org/10.1021/acsomega.2c04188
ACS Omega 2022, 7, 30571−30581

of nucleic acid (679, 786, and 826 cm^{-1}) in the 14 DIV hippocampal neuron group was significantly higher than that in the 7 DIV hippocampal neuron group ($P < 0.01$), and the content of collagen (859 cm^{-1}) was significantly higher in the 14 DIV hippocampal neuron group than in the 7 DIV hippocampal neuron group ($P < 0.01$) (Figure 2a,b).

We found that the amino acids screened by the OPLS model are mainly ketogenic and glycogenic amino acids (such as tryptophan, phenylalanine, and tyrosine), which are closely related to energy metabolism. Therefore, to further screen and distinguish the biological peaks of 7 DIV and 14 DIV hippocampal neurons, we selected the biological peaks corresponding to lipids and glucose-related to energy metabolism. We found that the contents of lipids (957, 1078, 1268, 1285, 1299, and 1437 cm^{-1}) and glucose (920 cm^{-1}) in the 14 DIV hippocampal neuron group were significantly higher than those in the 7 DIV hippocampal neuron group ($P < 0.01$) (Figure 2c).

Analysis of the Genes Involved in Hippocampal Neuron Development at Various Stages. The GSE113680 chip data yielded 340 DEGs in total, including 294 significantly downregulated DEGs and 46 significantly upregulated DEGs following the DEG screening conditions. Significantly upregulated genes are in red, and blue dots represent downregulated genes in the volcano plot (Figure 3a).

The DEGs were significantly enriched in 9 KEGG pathways, 38 GO-BP, 27 GO-CC, and 16 GO-MF. The top five GO function results were used for graphical representation after sorting the results based on P values from small to large (Figure 4 and Figure S2). Cell adhesion, chemical synaptic transmission, and intracellular signal transduction were the primary processes in BP; dendrites, nerve cell bodies, and axons were the primary components of CC; the Ras guanylate exchange factor activity, guanylate exchange factor activity, and enzyme binding function were the primary components of MF. According to KEGG analysis, the main signaling pathways for calcium, Ras, and cholinergic synaptic signals are involved in regulation (Figure 3c−f and Tables S3−S6).

There were 82 nodes and 109 interaction pairs in the PPI network. Key nodes of the network were those with a high topological score. In Figure S3 and Table S7, the top 10 genes' expression degree values and PPI network degree values are displayed, respectively. According to the findings, 14 DIV hippocampal neurons express these top 10 genes at a higher level than a group of 7 DIV hippocampal neurons. The cytohubba plug-in was used to verify the hub genes. The hub genes included the epidermal growth factor receptor (EGFR), protein tyrosine kinase 2-beta (PTK2B), ionotropic glutamate receptor NMDA-type subunit 2A (GRIN2A), tachykinin precursor 1 (TAC1), calcium/calmodulin-dependent protein kinase II-alpha (CAMK2A), discs large MAGUK scaffold protein 2 (DLG2), glutamate metabotropic receptor 5 (GRM5), Ras protein-specific guanine nucleotide releasing factor 1 (RASGRF1), potassium inwardly rectifying channel subfamily j member 4 (KCNJ4), and prostaglandin-endoperoxide synthase 2 (PTGS2). It was thought that they might interact strongly.

To screen biological peaks related to DEGs responsible for maturation, we screened the top 10 genes by informatics analysis, including receptor tyrosine kinase superfamily members, aspartate receptors, neuropeptide substance P, membrane-associated guanylate kinase, glutamate receptors, Ras guanine-releasing factors, and cyclooxygenase. The GO functional analysis of the top 10 genes revealed that the *PTK2B* gene was involved in cell adhesion; *GRIN2A*, *TAC1*, *DLG2*, and *GRM5* were involved in chemical synaptic transmission; *EGFR* and *RASGRF1* were involved in intracellular signal transduction; and *GRIN2A* and *RASGRF1* were involved in the regulation of synaptic plasticity. The genes for *PTK2B*, *TAC1*, *DLG2*, and *KCNJ4* mainly existed in dendrites, *PTK2B*, *TAC1*, *CAMK2A*, *DLG2*, *RASGRF1*, and *KCNJ4* in nerve cell bodies, *PTK2B*, *TAC1*, and *CAMK2A* in axons, *GRIN2A* and *GRM5* in dendritic ridges, and *EGFR*, *PTK2B*, *GRIN2A*, *TAC1*, *DLG2*, *GRM5*, *KCNJ4*, and *PTGS2* in cell membranes. The *RASGRF1* gene primarily encodes a guanylate exchange factor active molecule, *EGFR*, *PTK2B*, and *PTGS2* for an enzyme-binding molecule, *EGFR*, *PTK2B*, *TAC1*, *DLG2*, *GRM5*, and *RASGRF1* for a protein-binding molecule, and *GRIN2A*, *TAC1*, and *RASGRF1* for a glutamate receptor-binding molecule. The regulation of the calcium signaling pathway was affected by the genes *EGFR*, *PTK2B*, *GRIN2A*, *TAC1*, and *GRM5*; the regulation of the Ras signaling pathway was affected by the genes *EGFR*, *GRIN2A*, and *RASGRF1*, the regulation of the cholinergic synaptic signaling pathway by the genes *TAC1* and *KCNJ4*, the regulation of the oxytocin signaling pathway by the genes *EGFR*, *TAC1*, *KCNJ4*, and *PTGS2*, and the regulation of the insulin secretion signaling pathway by the gene *TAC1* (Figure 4a−d and Figure S2a−f). Next, to identify the main differential genes among the hub genes, we combined the findings of DEGs' GO functional analysis and regulatory pathway analysis with those of statistical analysis and the OPLS-DA model.

Combined with gene components, we further statistically analyzed the Raman spectrum data of hippocampal neuron supernatants. We found that, in the culture supernatant of 7 DIV and 14 DIV hippocampal neurons, the intensities of the tyrosine peak (643, 848, 897, 1603, and 1616 cm^{-1}) and guanine peak (1190, 1415, 1485, 1491, and 1573 cm^{-1}) in the 7 DIV hippocampal neuron group were significantly lower than in the 14 DIV hippocampal neuron group ($P < 0.01$) (Figure 2d,e). We screened the genes *EGFR*, *PTK2B*, *DLG2*, and *RASGRF1* related to tyrosine and guanine. Combined with the gene attributes and enrichment analysis results, it could be inferred that these four genes are the most likely differential genes involved in hippocampal neuronal maturation.

DISCUSSION

In this study, the NCBI.GEO database was used, and the expression profile data of hippocampal neurons of C57BL/6J mice cultured in vitro were compared with the Raman spectroscopy data of the supernatant of cells cultured in vitro to explore the typical characteristics of maturation. Neurons are highly differentiated post-mitotic cells, and the maturation of the brain is undoubtedly different from that of other organs. A single-cell whole-genome sequencing analysis showed that a single post-mitotic neuron in the human hippocampus undergoes somatic mutation with age. In the process of normal maturation, although the number of neurons will not reduce too much, the number, diameter, length, branches, and density of dendrites in neurons may decrease with age.[7,8] Humans have a higher risk of developing neurodegenerative diseases like Alzheimer's than other primates.[9] However, the mechanism of Alzheimer's disease also needs further research, and the clinical effects of the newly developed drugs are not satisfactory.[10] The pathogenesis of cognitive impairment diseases is closely related to the number

https://doi.org/10.1021/acsomega.2c04188
ACS Omega 2022, 7, 30571−30581

and structure of hippocampal neurons.[11] For normal neural activities to continue, the internal environment of the nervous system must be relatively stable. Many external factors can obstruct a cell's ability to function normally and cause cell damage. The cell adapts to environmental changes by activating a defense mechanism to prevent damage from noxious stimulations. Endogenous cytoprotection is a process that helps organisms maintain homeostasis in the internal environment. The self-defense mechanism has developed for long-term evolution. In this study, we investigated the internal environment of hippocampal neurons and combined cell culture experiments, Raman spectroscopy detection, multivariate analysis, and bioinformatics analysis.

Since the number, displacement, and length of Raman lines are directly related to the sample's molecular vibration or rotation energy level, we used this non-destructive and high-resolution imaging technology to detect the molecular vibration or rotation related to chemical bonds in the culture medium of hippocampal neurons. We learned more about the dynamic energy system of hippocampal neurons in the living cell survival environment during cell culture. It is crucial to study the neural environment.[12]

Mature hippocampal neurons need the energy to maintain their survival, excitability, and synaptic signal transmission under different behaviors. Hippocampal neurons use glucose as their main source of energy. Changes in lipid levels in the central nervous system also affect the glucose metabolism of hippocampal neurons in brain areas responsible for learning and memory.[13−16] Lipids also play an important role in hippocampal neuron plasticity, learning, and memory.[17] In this study, we found that the levels of ketogenic and glycogenic amino acids (tryptophan, phenylalanine, and tyrosine), lipid intake, and glucose utilization in the internal environment of 14 DIV neurons decreased. We infer that the levels of various ketogenic and glycogenic amino acids, lipids, and glucose are key factors in determining the energy utilization of mature neurons.

The relationship between the gene expression profile and disease is receiving more and more attention. We found that hippocampal neurons of various maturities have different energy metabolisms. Therefore, we downloaded and organized the gene microarray data from the gene expression omnibus (GEO) database related to the biological information analysis of hippocampal neurons. Then, we discussed the role of DEGs in the development and maturation of hippocampal neurons by analyzing DEGs to explore new therapeutic targets for the maturation and aging of hippocampal neurons. We used the GEO database to search for the "mouse hippocampal neurons in primary culture" as the keyword. After screening, it is submitted to GPL10740 by Stephan-Otto Attolini C. Sample data of two 0 DIV mouse hippocampal neurons (GSM3111025 and GSM3111031) are included in the GeneChip GSE113680 based on Affymetrix mouse gene 1.0 ST array (Figure S3).

We looked for genes that were differentially expressed between 0 and 15 DIV neurons through bioinformatics analysis, annotated the GO function of the differential genes, and performed KEGG pathway analysis. It was found that the differential genes were mainly involved in the BP of chemical synaptic transmission and intracellular signal transduction. The MF involved the Ras guanylate exchange factor and guanylate exchange factor. The Ras signaling pathway was the major regulated pathway. The epidermal growth factor receptor (EGFR), also known as ErbB1, is the first receptor tyrosine kinase superfamily member. EGFR exists in the adult cortex, cerebellum, and hippocampus neurons and is important for neuron growth and cell-surface signal transduction.[18−21] In the hippocampi of mice, the level of EGFR decreases with age.[18] Protein tyrosine kinase 2-beta (PTK2B) is a calcium-activated non-receptor tyrosine kinase. Genome-wide association analysis shows that *PTK2B* is closely related to Alzheimer's disease and is highly enriched in the hippocampus and part of the cerebral cortex pyramidal neurons. *PTK2B* accumulation is an early pathological marker of the disease and is a key component of the signaling pathway involved in axon growth and synapse formation.[22−24] *EGFR* and *PTK2B* genes are closely related to tyrosine metabolism. Therefore, we infer that maturation-related genes *EGFR* and *PTK2B* are of ketogenic and glycogenic amino acid metabolism and abnormal energy utilization and metabolism in mature neurons.

DLG2 belongs to the membrane-associated guanylate kinase family. It is an excitatory postsynaptic scaffold protein that interacts with synaptic surface receptors and signaling molecules. *DLG2* is widely expressed in the brain of adult rodents, including the cortex, hippocampus, striatum, and cerebellum. The lack of *DLG2* in the hippocampus leads to decreased long-term potentiation.[25,26] Ras protein-specific guanine-releasing factor 1 (RAS-GRF1) is a neuron-specific Ras protein guanine nucleotide exchange factor, which is only expressed in the brain and liver of newborns. It mediates neural plasticity through the Ras extracellular signal-regulated kinase (Ras−ERK) signaling pathway. *RAS-GRF1* regulates internal excitability, synaptic plasticity, and axon growth.[27−30] *DLG2* and *RAS-GRF1* are closely related to guanine metabolism. Guanine may be the key factor in determining the synaptic function of mature neurons.

The expression pattern of DEGs matches the changes in our peak levels of tyrosine and guanine. We speculate that changes in the levels of these proteins in the internal environment of mature neurons are responsible for their reduced ability to absorb external nutrients. In addition to directly degrading nutrients into useful substances, hippocampal neurons use simple substances to synthesize complex and important components. All proteins in life are composed of amino acids. When hippocampal neurons are cultured in a primary cell culture medium, they can synthesize all 20 amino acids from glucose and carbohydrates in the culture medium. When the culture medium already contains a substance, such as amino acid, the synthesis of that amino acid will stop rapidly because of the complex regulatory mechanism in biological cells. Thus, when there is a sufficient amount of a substance in the environment, the synthase enzyme for that substance will be specifically downregulated.[31,32] In this study, the levels of ketogenic and glycogenic amino acids (tryptophan, phenylalanine, and tyrosine), nucleic acids, collagen, lipids, and sugars contained in the culture supernatant of 14 DIV hippocampal neurons were higher than those in 7 DIV hippocampal neurons, suggesting that the synthetic process related to maintaining life energy and metabolic inheritance in 14 DIV cells was weakened or stopped, further confirming the "negative feedback" mechanism.

There are some limitations of this study. There are few studies on the sequencing of hippocampal neurons. In this study, we selected the embryonic hippocampus of pregnant day-17 mice (GSE113680) and hippocampal neurons on day 0 of in vitro culture as the data source for gene analysis of young

https://doi.org/10.1021/acsomega.2c04188
ACS Omega 2022, 7, 30571−30581

hippocampal neurons and the hippocampal neurons on day 15 of in vitro culture as the data source for gene analysis of mature hippocampal neurons. However, this data source was not identified as coming from C57BL/6J mice. The Gibco company provided the cell line selected in this study, and hippocampal neurons were isolated from C57BL/6J mouse embryos on day 17 of pregnancy. We selected culture supernatants of hippocampal neurons cultured for 0, 7, and 14 days as the research object, which did not match the data source of biological analysis in a strict sense. We adopted this experimental design because we hoped to explore the changes in the intracellular environment specifically related to maturation.[33,34] Too short of a cell culture time will not be conducive to the analysis of components. The cells cultured for 0 days can be identified as the youngest hippocampal neurons, which will help us to explore the differential genes related to maturation in this study. Raman technology has some drawbacks as well. This technology has not been widely adopted because of its relatively low signal-to-noise ratio, complicated spectral interpretation, lengthy shooting time, and spectral information processing program.

In conclusion, the decrease in tyrosine uptake in a ketogenic environment and glycogenic amino acids in the internal environment of mature neurons may be related to the expression of maturation-related genes *EGFR* and *PTK2B*. The decrease in guanine uptake in a nucleic acid-rich medium may be associated with the expression of maturation-related genes *DLG2* and *RASGRF1*. The utilization levels of ketogenic and glycogenic amino acids, collagen, lipids, and glucose decreased, which may be related to the abnormal energy utilization and metabolism of hippocampal neurons. The decrease in nucleic acid intake may be associated with synaptic failure. Raman spectroscopy will be used to interpret the heterogeneity of the internal environment of hippocampal neurons in the maturation process, which will help us to understand better the energy dynamic information molecules of hippocampal neurons and the environmental changes of metabolic communication. Intervention in the internal environment and metabolic signal level may be a possible way to alleviate the degeneration of neurons, laying a foundation for further investigation into the path.

METHODS

Establishment and Grouping of C57BL/6J Mouse Hippocampal Neurons Cultured in Vitro. Day-17 C57BL/6J mouse embryos were used to isolate Gibco primary mouse hippocampus neurons (catalog no. A15587, 1×10^6 viable cells/vial). Cryopreservation makes the hippocampal neurons extremely fragile, and they cannot be centrifuged. Therefore, it is advisable to not centrifuge the cells before inoculation, and the cell viability should be determined by the manual (i.e., hemocytometer) counting method. The pre-warmed (37 °C) complete Neurobasal/B-27 medium was rinsed across a poly-D-lysine-coated (4.5 μg/cm^2) culture plate before 0.5×10^6 live cells per well of the complete medium were added. The cells were incubated at 36−38 °C in an environment humidified with air containing 5% CO_2. Half of the medium was removed from the culture hole and replaced with fresh medium after 24 h. Because neurons must be strictly cultured as an adherent culture and cannot be exposed to air, the cells were fed every third day by aspirating half of the medium from each well and replacing it with fresh medium until 14 days of culture. The control group consisted of mouse hippocampal neurons cultured in vitro for 0 days (0 DIV), while the experimental group included normal cultured mouse neurons cultured for 7 days (7 DIV) and 14 days (14 DIV).

Raman Spectroscopy. First, the supernatant of the cell culture was obtained by centrifugation to remove the suspended particles and then kept aside. Hippocampal neurons from 0, 7, and 14 DIVs had their culture supernatant (5 μL) dropped on a quartz glass slide for analysis using a confocal Raman spectrometer (XploRA Raman microscope). The parameters were as follows: laser excitation wavelength of 785 nm, output power of 10 mW, and objective lens at 40×. On the three-dimensional platform, the specimen was fixed. A Nikon camera with a 40× lens (0.6 numerical aperture) was used to take pictures. The detection wavelength range was 600−1800 cm^{-1}. For each group, 29−30 sites were examined. The resolution was 1 cm^{-1}. Data-processing tasks like baseline correction and smoothing were performed using Labspec6 software. The 1450 cm^{-1} Raman peaks in each spectrum served as internal standards for normalization.

Establishment of a Discrimination Model of 0, 7, and 14 DIV Hippocampal Neurons Using Orthogonal Partial Least Squares Discriminant Analysis (OPLS-DA). For the OPLS-DA of Raman spectroscopy data for the culture medium of 0, 7, and 14 DIV hippocampal neurons, SIMCA14.1 software was used. The effectiveness of the OPLS model was assessed using the fitting parameters R^2 and Q^2. The model was resampled 200 times under a null hypothesis using a random Y matrix change. We performed a receiver operating characteristic (ROC) curve analysis and cluster analysis. The $V + S$ analysis, which chose peaks with variable importance (VIP) of >1.5 and P (corr) of >0.4 as potential biomarkers, was used to identify statistically significant Raman peaks in the classification model as potential biomarkers. The obtained potential biomarkers underwent statistical analysis, and those with a $P < 0.05$ were considered statistically significant. The processing of pertinent data was done using Origin software.

A supervised dimensionality reduction technique called supervised OPLS-DA uses two- and three-dimensional score diagrams to depict the sample distribution, correlation, separation trend, and the overall state of the data set. It was used to identify variables that significantly differ between groups using supervised OPLS-DA analysis. Orthogonal signal correction (OSC) and partial least squares (PLS) can be combined with OPLS-DA to correct data. OSC can eliminate the influence of variables like diet and environment and reduce the heterogeneity of clinical samples by using metabonomics technology in clinical research. In a given data set X, OPLS eliminates the system orthogonal variables and distinguishes them from non-orthogonal variables, which can be analyzed independently. The OPLS method divides X into three parts as follows using data from the response variable y

$$X = T_P P^T{}_P + T_O P^T{}_O + E$$

where T_P represents the predicted score matrix of X, $P^T{}_P$ represents the predicted load matrix of X, $T_P P^T{}_P$ represents the expected part, T_O represents the score matrix of the orthogonal component of X and Y (called OPLS component), $P^T{}_O$ represents the corresponding load matrix, $T_O P^T{}_O$ represents the part orthogonal to Y, and E is the residual matrix.

The OPLS method is implemented in two steps:

The first step is to eliminate the variables orthogonal to Y from the X data matrix, that is

https://doi.org/10.1021/acsomega.2c04188
ACS Omega 2022, 7, 30571−30581

$$X_P = X - T_O P^T{}_O$$

where T_O is the score matrix of the component orthogonal to Y and $P^T{}_O$ is the load matrix corresponding to it.

The second step is a partial least squares analysis of X_P.

Screening of Differentially Expressed Genes (DEGs) between Hippocampal Neurons Cultured at Various Durations. *Data Source.* The NCBI gene expression omnibus (GEO, http://www.ncbi.nlm.nih.gov/geo/), which contains two samples of mouse hippocampal neurons cultured for 0 days and two samples of mouse hippocampal neurons cultured for 15 days and both of which provide expression profile data, was used to extract the data. The serial data number for this database is GSE113680 (species: *Mus musculus*). All samples were found on the GPL10740 Affymetrix Mouse Gene 1.0 ST array platform.

DEG Analysis. Analysis was performed using the GEO database's online analysis tool, GEO2R. To screen for DEGs between 0 DIV and 14 DIV hippocampal neurons with $P < 0.05$ and $|\log FC| > 4$, GEO2R uses the R language packages GEOquery and limma.

Functional Analysis of DEGs. Gene ontology (GO) functional annotation was done using the database for annotation, visualization, and integration discovery online analysis tool (https://david.ncifcrf.gov/), and Kyoto Encyclopedia of Genes and Genomes (KEGG) signal pathway enrichment analyses were done to analyze the DEGs. The biological process (BP), cellular component (CC), and molecular function (MF) are the three main aspects of GO function.

Protein−Protein Interaction (PPI) Network and Hub Gene Analysis. The relationship between proteins encoded by various genes was examined using the protein−protein interaction database STRING11.0 (https://sring-db.org/). The PPI results were examined using Cytoscape software, and the network's nodes' scores were examined using the network topology property index degree centrality. The likelihood in that a node is a key node increases with the node score. Genes with high network connectivity were hub genes and corresponded to the top 10 proteins (degree.-TOP10) in the PPI network nodes.

Statistical Analysis. The corresponding peaks of potential biomarkers identified by OPLS-DA were confirmed using statistical methods as were the biologically significant peaks associated with the differential genes of hippocampal neurons after varying the culture duration. IBM SPSS Statistics 26 was used for statistical analysis to verify the OPLS results and the biological peaks related to the DEGs. Normally distributed data are expressed as mean ± standard deviation (SD) ($x \pm s$). Intergroup comparisons were made using a one-way analysis of variance. In contrast, comparisons between homogeneous variance groups were made using the least significant difference method, and comparisons between groups with uneven variance were made using Tamhane's T2 method. When data were not normally distributed, they were expressed as the median (interquartile interval), and the Kruskal−Wallis test was used to compare the group differences. Statistical significance was defined as $P < 0.05$. GraphPad Prism 6 was used to prepare all graphs in this article.

■ ASSOCIATED CONTENT

Supporting Information

The Supporting Information is available free of charge at https://pubs.acs.org/doi/10.1021/acsomega.2c04188.

Flow chart for deciphering the heterogeneity of the internal environment of hippocampal neurons during maturation, gene ontology function and regulatory signal pathway analysis of the top 10 genes of 0 DIV and 15 DIV hippocampal neurons, degree value of screened key differential candidate genes, establishment of the OPLS-DA model, Raman spectra of culture supernatant for the 0 DIV group, 7 DIV group, and 14 DIV groups, DEGs identified in GSE113680, DEGs identified in GSE113680, top five data of biological process enrichment analysis, top five data of cellular component enrichment analysis, top 5 data of molecular function enrichment analysis, top 5 data of KEGG pathway enrichment analysis, PPI network degree value top 10 list of DEGs, and screened statistically significant potential biomarker peaks (PDF)

■ AUTHOR INFORMATION

Corresponding Authors

Min Gong − *Department of Pharmacy, Tianjin Medical University, Tianjin 300070, China*; Email: gongmin@tmu.edu.cn

Yuan Zhou − *State Key Laboratory of Experimental Hematology, National Clinical Research Center for Blood Diseases, Haihe Laboratory of Cell Ecosystem, Institute of Hematology and Blood Diseases Hospital, Chinese Academy of Medical Sciences & Peking Union Medical College, Tianjin 300020, China*; Email: yuanzhou@ihcams.ac.cn

Qiang Zhang − *Department of Geriatrics, Tianjin Medical University General Hospital, Tianjin Geriatrics Institute, Tianjin 300052, China*; Email: zhangqiangyulv@163.com

Authors

Xiaodong Kong − *Department of Geriatrics, Tianjin Medical University General Hospital, Tianjin Geriatrics Institute, Tianjin 300052, China*

Haoyue Liang − *State Key Laboratory of Experimental Hematology, National Clinical Research Center for Blood Diseases, Haihe Laboratory of Cell Ecosystem, Institute of Hematology and Blood Diseases Hospital, Chinese Academy of Medical Sciences & Peking Union Medical College, Tianjin 300020, China*; orcid.org/0000-0002-3766-7605

Kexuan Zhou − *Department of Geriatrics, Tianjin Medical University General Hospital, Tianjin Geriatrics Institute, Tianjin 300052, China*

Haoyu Wang − *State Key Laboratory of Experimental Hematology, National Clinical Research Center for Blood Diseases, Haihe Laboratory of Cell Ecosystem, Institute of Hematology and Blood Diseases Hospital, Chinese Academy of Medical Sciences & Peking Union Medical College, Tianjin 300020, China*

Dai Li − *Department of Geriatrics, Tianjin Medical University General Hospital, Tianjin Geriatrics Institute, Tianjin 300052, China*

Shishuang Zhang − *Department of Geriatrics, Tianjin Medical University General Hospital, Tianjin Geriatrics Institute, Tianjin 300052, China*

https://doi.org/10.1021/acsomega.2c04188
ACS Omega 2022, 7, 30571−30581

Ning Sun − *Department of Geriatrics, Tianjin Medical University General Hospital, Tianjin Geriatrics Institute, Tianjin 300052, China*

Complete contact information is available at: https://pubs.acs.org/10.1021/acsomega.2c04188

Author Contributions

#X.K. and H.L. contributed equally to this work. Q.Z. and Y.Z. were involved in the study concept and design. X.K., H.L., K.Z., H.W., D.L., S.Z., and N.S. were involved in the data acquisition, analysis, interpretation, drafting, and preparation of the manuscript.

Funding

This work was supported by grants from the National Natural Science Foundation of China (grant nos. 81970085 and 81970120) and the Tianjin Science and Technology Plan Project (grant no. 18ZXDBSY00090). This work was partly supported by the Tianjin Health and Health Committee Foundation (grant no. ZC20184). This work was supported and funded by the Tianjin Key Medical Discipline (Specialty) Construction Project (grant no. TJYXZDXK-006A).

Notes

The authors declare no competing financial interest.

■ ACKNOWLEDGMENTS

The authors would like to thank the core facilities of the State Key Laboratory of Experimental Hematology, Institute of Hematology and Blood Diseases Hospital, and Chinese Academy of Medical Sciences and Peking Union Medical College for their technical assistance.

■ REFERENCES

(1) Berg, D. A.; Su, Y.; Jimenez-Cyrus, D.; Patel, A.; Huang, N.; Morizet, D.; Lee, S.; Shah, R.; Ringeling, F. R.; Jain, R.; Epstein, J. A.; Wu, Q. F.; Canzar, S.; Ming, G. L.; Song, H.; Bond, A. M. A common embryonic origin of stem cells drives developmental and adult neurogenesis. *Cell* **2019**, *177*, 654−668.e15.

(2) Zeisel, A.; Muñoz-Manchado, A. B.; Codeluppi, S.; Lönnerberg, P.; La Manno, G.; Juréus, A.; Marques, S. Brain structure. Cell types in the mouse cortex and hippocampus revealed by single-cell RNA-seq. *Science* **2015**, *347*, 1138−1142.

(3) Wang, H. Q.; Wu, H. . Q.; Yu, X. R. Research advances on neural cell senescence and cellular senescence models. *Chin. J. Geriatr.* **2020**, *39*, 600−604. (in Chinese)

(4) Sparkman, N. L.; Johnson, R. W. Neuroinflammation associated with aging sensitizes the brain to the effects of infection or stress. *NeuroImmunoModulation* **2008**, *15*, 323−330.

(5) Tay, T. L.; Savage, J. C.; Hui, C. W.; Bisht, K.; Tremblay, M. È. Microglia across the lifespan: from origin to function in brain development, plasticity and cognition. *J. Physiol.* **2017**, *595*, 1929−1945.

(6) Liang, H.; Cheng, X.; Dong, S.; Wang, H.; Liu, E.; Ru, Y.; Li, Y.; Kong, X.; Gao, Y. Rapid and non-invasive discrimination of acute leukemia bone marrow supernatants by Raman spectroscopy and multivariate statistical analysis. *J. Pharm. Biomed. Anal.* **2022**, *210*, No. 114560.

(7) Isaev, N. K.; Stelmashook, E. V.; Genrikhs, E. E. Neurogenesis and brain aging. *Rev. Neurosci.* **2019**, *30*, 573−580.

(8) Stavoe, A. K. H.; Holzbaur, E. L. F. Autophagy in neurons. *Annu. Rev. Cell Dev. Biol.* **2019**, *35*, 477−500.

(9) Mertens, J.; Reid, D.; Lau, S.; Kim, Y.; Gage, Z. Aging in a dish: iPSC-derived and directly induced neurons for studying brain aging and age-related neurodegenerative diseases. *Annu. Rev. Genet.* **2018**, *52*, 271−293.

(10) Breijyeh, Z.; Karaman, R. Comprehensive review on Alzheimer's disease: causes and treatment. *Molecules* **2020**, *25*, 5789.

(11) Williamson, L. L.; Bilbo, S. D. Chemokines and the hippocampus: A new perspective on hippocampal plasticity and vulnerability. *Brain Behav. Immun.* **2013**, *30*, 186−194.

(12) Payne, T. D.; Moody, A. S.; Wood, A. L.; Pimiento, P. A.; Elliott, J. C.; Sharma, B. Raman spectros-copy and neuroscience:from fundamental understanding to disease diagnostics and imaging. *Analyst* **2020**, *145*, 3461−3480.

(13) Beckervordersandforth, R.; Ebert, B.; Schäffner, I.; Moss, J.; Fiebig, C.; Shin, J.; Moore, D. L.; Ghosh, L.; Trinchero, M. F.; Stockburger, C.; Friedland, K.; Steib, K.; von Wittgenstein, J.; Keiner, S.; Redecker, C.; Hölter, S. M.; Xiang, W.; Wurst, W.; Jagasia, R.; Schinder, A. F.; Ming, G. L.; Toni, N.; Jessberger, S.; Song, H.; Lie, D. C. Role of mitochondrial metabolism in the control of early lineage progression and aging phenotypes in adult hippocampal neurogenesis. *Neuron* **2017**, *93*, 560−573.e6.

(14) Uddin, M. M.; Ibrahim, M. M. H.; Aryal, D.; Briski, K. P. Sex-dimorphic moderate hypoglycemia preconditioning effects on Hippocampal CA1 neuron bio-energetic and anti-oxidant function. *Mol. Cell. Biochem.* **2020**, *473*, 39−50.

(15) Cisternas, P.; Martinez, M.; Ahima, R. S.; William Wong, G.; Inestrosa, N. C. Modulation of glucose metabolism in hippocampal neurons by adiponectin and resistin. *Mol. Neurobiol.* **2019**, *56*, 3024−3037.

(16) Dartora, C. M.; Borelli, W. V.; Koole, M.; Marques da Silva, A. M. Cognitive decline assessment: a review from medical imaging perspective. *Front. Aging Neurosci.* **2021**, *13*, 502.

(17) Malikovic, J.; Vuyyuru, H.; Koefeler, H.; Smidak, R.; Höger, H.; Kalaba, P. Moderate differences in common feeding diets change lipid composition in the hippocampal dentate gyrus and affect spatial cognitive flexibility in male rats. *Neurochem. Int.* **2019**, *128*, 215−221.

(18) Romano, R.; Bucci, C. Role of EGFR in the Nervous System. *Cell* **2020**, *9*, 1887.

(19) Chen, H.; Liu, B.; Neufeld, A. H. Epidermal growth factor receptor in adult retinal neurons of rat, mouse, and human. *J. Comp. Neurol.* **2007**, *500*, 299−310.

(20) Stateva, S. R.; Salas, V.; Benguría, A.; Cossío, I.; Anguita, E.; Martín-Nieto, J.; Benaim, G.; Villalobo, A. The activating role of phospho-(Tyr)-calmodulin on the epidermal growth factor receptor. *Biochem. J.* **2015**, *472*, 195−204.

(21) Wang, L.; Liang, B.; Zhong, Y. Reduced EGFR level potentially mediates the Aβ42-induced neuronal loss in transgenic fruit fly and mouse. *Protein Cell* **2013**, *4*, 647−649.

(22) Giralt, A.; de Pins, B.; Cifuentes-Díaz, C.; López-Molina, L.; Farah, A. T.; Tible, M.; Deramecourt, V.; Arold, S. T.; Ginés, S.; Hugon, J.; Girault, J. A. PTK2B/Pyk2 overexpression improves a mouse model of Alzheimer's disease. *Exp. Neurol.* **2018**, *307*, 62−73.

(23) de Pins, B.; Mendes, T.; Giralt, A.; Girault, J. A. The non-receptor tyrosine kinase pyk2 in brain function and neurological and psychiatric diseases. *Front Synaptic Neurosci.* **2021**, *13*, No. 749001.

(24) Dourlen, P.; Fernandez-Gomez, F. J.; Dupont, C.; Grenier-Boley, B.; Bellenguez, C.; Obriot, H.; Caillierez, R.; Sottejeau, Y.; Chapuis, J.; Bretteville, A.; Abdelfettah, F.; Delay, C.; Malmanche, N.; Soininen, H.; Hiltunen, M.; Galas, M. C.; Amouyel, P.; Sergeant, N.; Buée, L.; Lambert, J. C.; Dermaut, B. Functional screening of Alzheimer risk loci identifies PTK2B as an in vivo modulator and early marker of Tau pathology. *Mol. Psychiatry* **2017**, *22*, 874−883.

(25) Yoo, T.; Kim, S. G.; Yang, S. H.; Kim, H.; Kim, E.; Kim, S. Y. A DLG2 deficiency in mice leads to reduced sociability and increased repetitive behavior accompanied by aberrant synaptic transmission in the dorsal striatum. *Mol. Autism* **2020**, *11*, 19.

(26) Keane, S.; Martinsson, T.; Kogner, P.; Ejeskär, K. The loss of DLG2 isoform 7/8, but not isoform 2, is critical in advanced staged neuroblastoma. *Cancer Cell Int.* **2021**, *21*, 170.

(27) Chen, X.; Peng, X.; Wang, L.; Fu, X.; Zhou, J. X.; Zhu, B.; Luo, J.; Wang, X.; Xiao, Z. Association of RASGRF1 methylation with epileptic seizures. *Oncotarget* **2017**, *8*, 46286−46297.

(28) Abarzua, S.; Ampuero, E.; van Zundert, B. Superoxide generation via the NR2B-NMDAR/RASGRF1/NOX2 pathway promotes dendritogenesis. *J. Cell. Physiol.* **2019**, *234*, 22985−22995.
(29) Tonini, R.; Franceschetti, S.; Parolaro, D.; Sala, M.; Mancinelli, E.; Tininini, S.; Brusetti, R.; Sancini, G.; Brambilla, R.; Martegani, E.; Sturani, E.; Zippel, R. Involvement of CDC25Mm/RAS-GRF1-dependent signaling in the control of neuronal excitability. *Mol. Cell Neurosci.* **2001**, *18*, 691−701.
(30) D'Isa, R.; Clapcote, S. J.; Voikar, V.; Wolfer, D. P.; Giese, K. P.; Brambilla, R. Mice lacking RAS-GRF1 show contextual fear conditioning but not spatial memory impairments: convergent evidence from two independently generated mouse mutant lines. *Front Behav. Neurosci.* **2011**, *5*, 78.
(31) Rose, A. J. Amino acid nutrition and metabolism in health and disease. *Nutrients* **2019**, *11*, 2623.
(32) Radulescu, C. I.; Cerar, V.; Haslehurst, P.; Kopanitsa, M.; Barnes, S. J. The aging mouse brain: cognition, connectivity and calcium. *Cell Calcium* **2021**, *94*, No. 102358.
(33) Lesuisse, C.; Martin, L. J. Long-term culture of mouse cortical neurons as a model for neuronal development, aging, and death. *J. Neurobiol.* **2002**, *51*, 9−23.
(34) Strother, L.; Miles, G. B.; Holiday, A. R.; Cheng, Y.; Doherty, G. H. Long-term culture of SH-SY5Y neuroblastoma cells in the absence of neurotrophins: A novel model of neuronal ageing. *J. Neurosci Methods* **2021**, *362*, No. 109301.

https://doi.org/10.1021/acsomega.2c04188
ACS Omega 2022, 7, 30571−30581